Available online at www.sciencedirect.com
SCIENCE DIRECT®
Scripta Materialia 53 (2005) 845–850
Scripta MATERIALIA
www.actamat-journals.com

Transmission electron microscopy of cold sprayed 1100 aluminum coating

K. Balani [a], A. Agarwal [a,*], S. Seal [b], J. Karthikeyan [c]

[a] Department of Mechanical and Materials Engineering, Florida International University, EC 3464, 10555 West Flagler Street, Miami, FL 33174, United States
[b] Advanced Material Process and Analysis Center (AMPAC), Department of Mechanical, Materials and Aerospace Engineering (MMAE), University of Central Florida, Eng 381, 4000 Central Florida Blvd, Orlando, FL 32826, United States
[c] ASB Industries Inc., Barberton, OH 44203, United States

Received 28 February 2005; received in revised form 11 April 2005; accepted 3 June 2005
Available online 6 July 2005

Abstract

Cold-spraying of 1100 Al powder particles onto 1100 Al substrate was accomplished using carrier gases 100 vol.% He and a mixture of He–20 vol.% N_2. TEM characterization correlates very well the occurrence of dislocations, presence of oxide, and surface instability phenomenon with observed mechanical and corrosion properties of the cold-sprayed coating.

Keywords: Cold spraying; 1100 Aluminum coating; TEM

1. Introduction

In the 1990s, the cold spraying process emerged in North America, having been developed in the mid-1980s by the Siberian Division of the Russia Academy at the Institute of Theoretical and Applied Mechanics [1–3]. A high-pressure ($\sim 3.5 \times 10^6$ N/m^2) supersonic gas jet is utilized for accelerating fine powder particles to above a critical velocity ($\sim$500–1200 m/s), to deposit them as coatings [1–8]. The kinetic energy subsequently dispensed during the impact of the powder particle with the substrate ruptures the surface oxide, plastically deforms the particle and it approaches the clean surface of the substrate, thereby bonding particle as a deposition coating [9].

In our earlier work, 100 vol.% helium (He) and a mixture of helium and 20 vol.% nitrogen (He–20 vol.% N_2) were used as carrier gases for depositing 1100 Al onto 1100 Al substrate via the cold spray technique [3]. The higher sonic velocity and higher degree of tamping in 100 vol.% He when compared to that of He–20 vol.% N_2 carrier gas resulted in denser and harder coatings [3,10]. The addition of N_2, being a diatomic gas, into He increased the enthalpy of the carrier gas for better heat-transfer with spray particles [11]. However, addition of N_2 in He reduced the velocity of sprayed particles due to the heavier atomic mass resulting in coatings with reduced density and hardness [3]. Also, 100 vol.% He processed coating displayed inferior corrosion resistance when compared to that of He–20 vol.% N_2 at 0.9 pH using sulfuric acid (H_2SO_4) as an electrolyte [3]. Both the cold-sprayed coatings were more corrosion resistant compared to the 1100 Al substrate.

In the present study, high magnification scanning electron microscopy (SEM) and transmission electron microscopy (TEM) were utilized to elucidate and substantiate results and findings of our earlier work [3]. TEM imaging educed dislocation piling, surface

* Corresponding author. Tel.: +1 305 348 1701; fax: +1 305 348 1932.
E-mail address: agarwala@fiu.edu (A. Agarwal).

1359-6462/$ - see front matter © 2005 Acta Materialia Inc. Published by Elsevier Ltd. All rights reserved.
doi:10.1016/j.scriptamat.2005.06.008

morphology and subgrain structure describing the degree of strain hardening, hardness, and resulting propensity of chemical attack under electrochemical studies. These advanced analytical techniques provide for better understanding, enabling correlations to be made between the microstructure and the microhardness properties and electrochemical behavior of cold sprayed 1100 Al coating [3,12].

2. Experimental details

Cold spraying of fine (1–30 μm) and spherical 1100 Al powders onto similar substrate ($300 \times 75 \times 5\ mm^3$) was performed using a converging–diverging nozzle at ASB Industries, Ohio. Preheated powders (500–800 K) were accelerated using high pressure carrier gas ($\sim 2.1 \times 10^6\ N/m^2$) for deposition onto the 1100 Al substrate. Density measurements, coating morphological studies, micro hardness testing and electrochemical analysis have been detailed in our earlier paper [3].

SEM characterization was carried out using a JEOL JSM 6330 F field emission electron microscope. TEM analysis for as-received powder involved suspending Al powders in acetone, ultrasonicating for 10 min, dipping copper grid in the solution, drying for 10 min and inserting in vacuum chamber for an hour before inserting the sample in the TEM chamber. For sample extraction from the two differently processed 1100 Al coatings, an FEI focused ion beam 200 TEM field emission magnum column workstation with a gallium liquid metal ion source was used. The details of the TEM sample preparation technique has been described elsewhere [13,14]. TEM studies were carried using FEI Tecnai F30 TEM operating at a voltage of 300 kV.

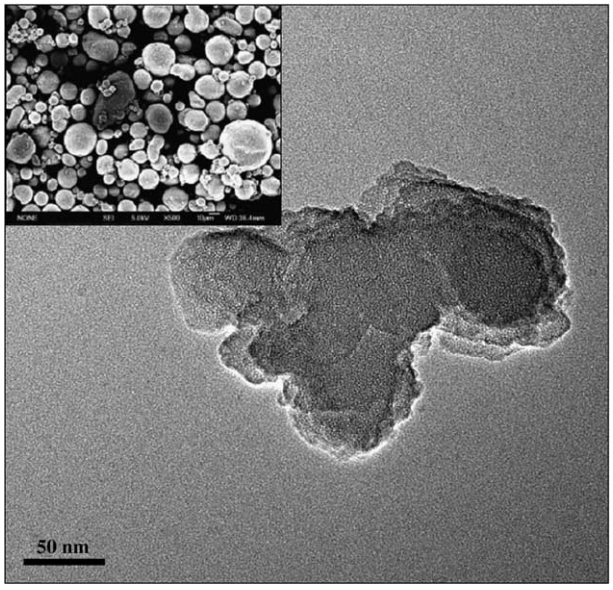

Fig. 1. TEM image of as-received 1100 Al powder particle.

3. Results and discussions

3.1. As-received 1100 Al

As seen in Fig. 1, as-received 1100 Al powder particles were spherical and in the size range of 1–30 μm, with a mean free size of 6.5 μm [3]. The TEM image, Fig. 1, clearly depicts a typical crystallite size in the range of ~200 nm for as-received 1100 Al powder particle. Fig. 1 elicits that starting powder grains are relaxed and not stressed, and therefore possess low dislocation density. A comparison of starting powder to synthesized coating, discussed later in this paper, distinguishes the implication of surface relief and dislocation piling towards explaining the hardness and electrochemical behavior of cold sprayed coatings.

3.2. Microstructural characterization of deposited coating

3.2.1. Structural features and morphology

The deposited 1100 Al coatings onto 1100 Al substrate, using 100 vol.% He and a mixture of He–20 vol.% N_2, have been characterized and compared for relative microstructural behavior [3]. A high magnification SEM image, Fig. 2, shows the rigid and stressed but smooth structure of unetched 100 vol.% He processed 1100 Al coating. The coating exhibits river marking showing its brittle nature. These flat facets generally form via local deformation, relating to the quasi-cleavage nature of the coating [15]. Shock wave flow-lines in the 100 vol.% He processed coating indicate that the material underwent sudden local deformation in a restricted period, generating higher strain hardening of the sprayed structure. This occurs since the high velocity-impacts of spray particles do not allow much time for the particles to deform, immediately following

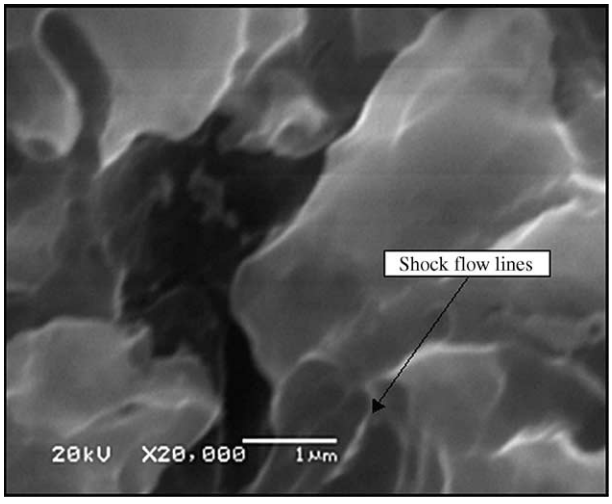

Fig. 2. High magnification SEM image showing shock flow lines in 100 vol.% He sprayed 1100 Al coating.

the deposition of the next layer of particles [6]. This restricted relaxation time after the deposition, in turn, leaves high strain hardening and hence higher hardness in the deposited coating.

Fig. 3 displays ridges and valleys in the microstructure, implying highly deformed surfaces in the He–20 vol.% N_2 sprayed 1100 Al coating. Craters and submicron pores endorse multiple impacts onto the deposition surface, leading to a higher degree of flattening. Addition of nitrogen in helium causes a reduction in sonic velocity and thereby generates a time lag between the successive splat depositions when compared to helium alone as carrier gas. This phenomenon of non-deposition (or multiple) impacts of spray particles led to splat size enlargement [3]. Thereby, He–20 vol.% N_2 processed coating displayed a bigger splat size when compared to that of 100 vol.% He processed coating.

3.2.2. Interfacial curvature and instability phenomenon

Perturbations and differential velocities at the deforming splat interface can be explained by Kelvin–Helmholtz instability phenomena via reckoning and duration of successive impacts during the plastic deformation of cold-sprayed coating [8]. The centrifugal force generated due to the plastic flow at the interface produces differential interfacial velocities. Differential interfacial velocities perturb the flow and generate centrifugal force giving non-zero curvature along the interface, as shown schematically in Fig. 4. Perturbations occur even when the density of substrate and coating material is the same [8]. The varying intensity of impacts for 100 vol.% He, and the mixture of He–20 vol.% N_2 carrier gases will therefore have contrasting interfacial perturbations. Also, it may obviously be expected that Kelvin–Helmholtz instability phenomenon will dominate at the interfacial layer towards mechanically interlocking the adjacent surfaces [8]. The substrate/coating interface impact-fusion model is also described elsewhere [16,17]. The following TEM analysis effectively relates the interfacial perturbations to the mechanical and corrosion properties of the cold-sprayed coatings.

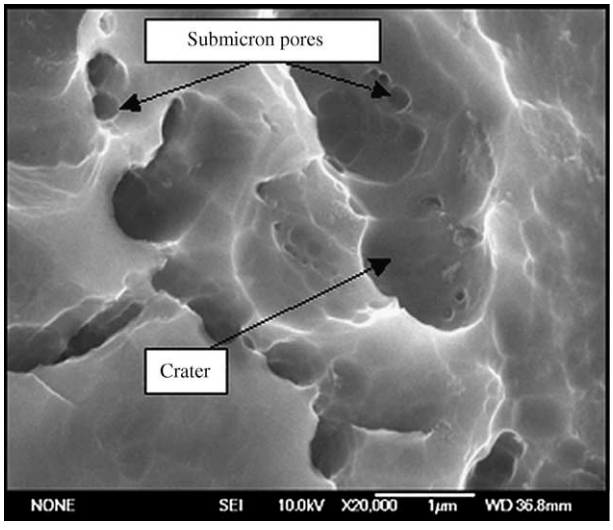

Fig. 3. High magnification SEM image showing ridges and valleys in He–20 vol.% N_2 sprayed 1100 Al coating.

3.2.3. Influence of surface oxidation onto mechanical and corrosion properties

Deposition of 1100 Al using 100 vol.% He evidently shows generation of oxide layer at the interface of splats, Fig. 5, due to high reactivity of the surface of the preheated powder. Moreover, generation of ceramic oxide onto the surface, therefore, substantiates the higher hardness values on the cold-sprayed 1100 Al coating [3]. But, on the other hand, the concentration of oxide generates potential site for active corrosion under electrochemical studies. Hence a higher degree of strain-confinement and polarized sites may also lead to higher critical corrosion current densities, which indeed is the case [3].

TEM image, Fig. 6, of He–20 vol.% N_2 sprayed Al coating captured wave-flow pattern, implying that mechanical bonding between the layers of deposited particles is attributed to shear instabilities as explained earlier in Fig. 4 [6,8,18]. Availability of sufficient time to flow, assisted with impacts from non-depositing spray particles, help further integration of the flow lines in the coating. Hence it can be estimated that surface oxide will rupture from the multiple impacts of non-depositing

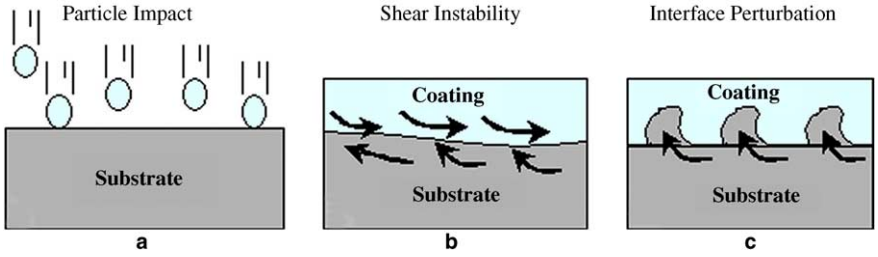

Fig. 4. Schematic of the curvature generation along interface; (a) particles impacting onto surface, (b) differential flow velocities along interface, (c) generation of interface curvature.

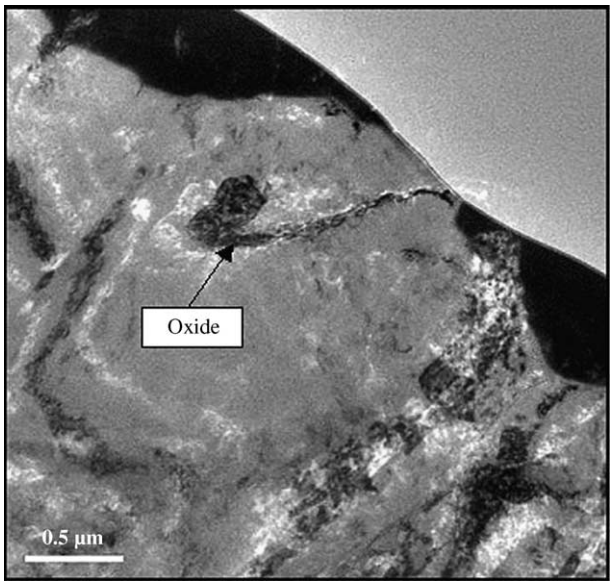

Fig. 5. TEM image of 100 He processed 1100 Al coating showing oxide layer.

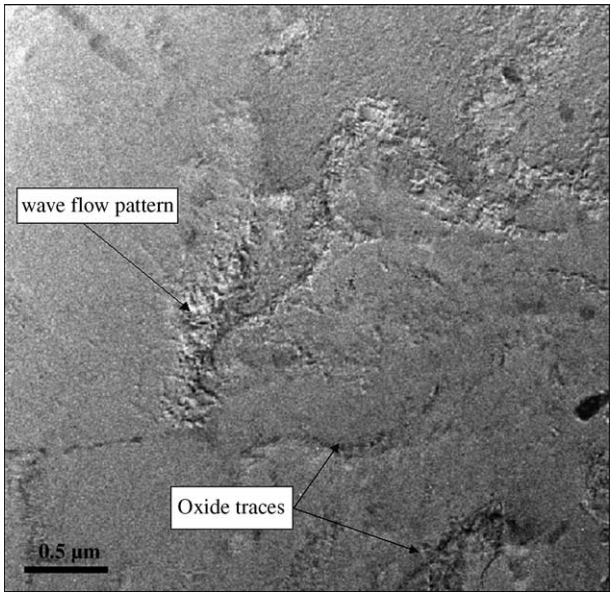

Fig. 6. TEM image of He–20 vol.% N_2 1100 Al coating showing wave flow pattern.

particles. This justifies the presence of ruptured traces of oxides visible in Fig. 6. Helium gas is lighter (0.1785 kg/m^3) than air, hence a higher sonic velocity (or a higher degree of impact) raises the temperature compared with the addition of nitrogen in the carrier gas [2,3,5,6]. Hence, the generation of oxide is more probable in He-processed coating. Owing to the fact that multiple non-depositing impacts (similar to shot-peening) occur under He–20 vol.% N_2 processing to break oxides, no significant oxidation of surface was observed in the micrograph, Fig. 6.

3.2.4. Subgrain rearrangement and dislocation piling

The low degree of rearrangement in 100 vol.% He processed coating, due to the quick deposition of the splats, restricts the wave-flow pattern, as observed in high magnification TEM images, Fig. 7. Also only smooth interfaces are observed in Fig. 7 since the degree of plastic deformation is limited to the time the next splat impacts and deposits onto the surface. The high carrying capacity of 100 vol.% He accelerates the 1100 Al powder particles rapidly above the critical velocity, but provides less time for reorientation before the next layer of particles are deposited [5,10]. Hence, the limited flow of relative surfaces restricts the high degree perturbations at interface. It may therefore be expected that a smooth transition will occur between depositing splats. The selected area diffraction pattern shown as an inset in Fig. 7 corresponds to aluminum.

The TEM image of He–20 vol.% N_2 processed 1100 Al coating, Fig. 8, elucidates the subgrain formation (120–250 nm), indicating stress relief in the deposited coating [18]. The subgrain structure indicates that He–20 vol.% N_2 coating has undergone a high degree of plastic deformation, and few dislocations are getting entangled in the cell walls. Reorientation of the structure endorses lower hardness values resulting from relieving the strain hardening effects of deposited particles [15,16,18].

100 vol.% He processed coatings showed constrained beach-sand marks under high magnification TEM images, indicating high stresses along wave edges. Hence restricted curvatures formation by redistribution of interfacial flow stresses generated dislocations during plastic deformation, as seen in Fig. 9. No ripples or ridges and the absence of subgrain formation imply

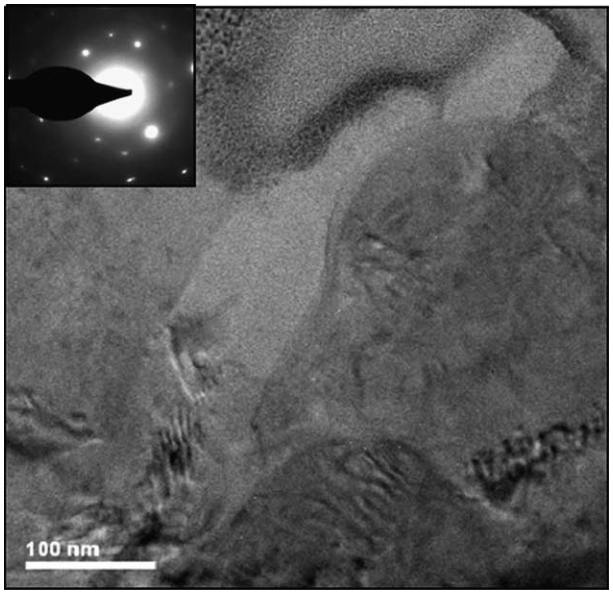

Fig. 7. TEM image of 100 vol.% He processed coating showing restricted wave flow at interface. Inset: SAED pattern for Al.

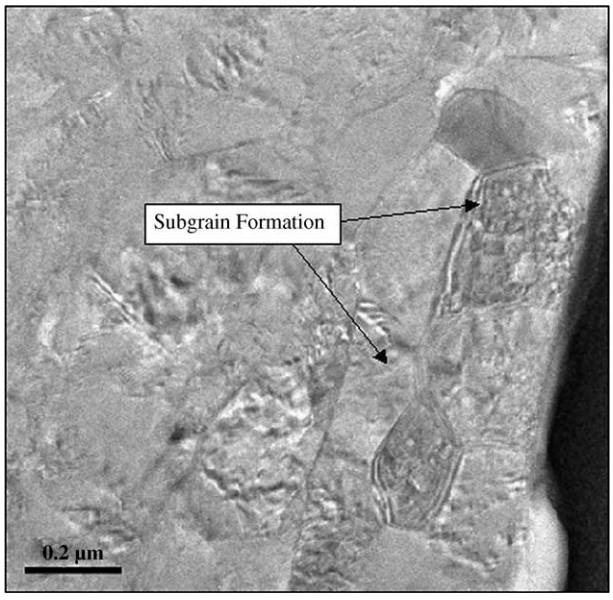

Fig. 8. TEM image of He–20 vol.% N_2 processed coating depicting subgrain formation.

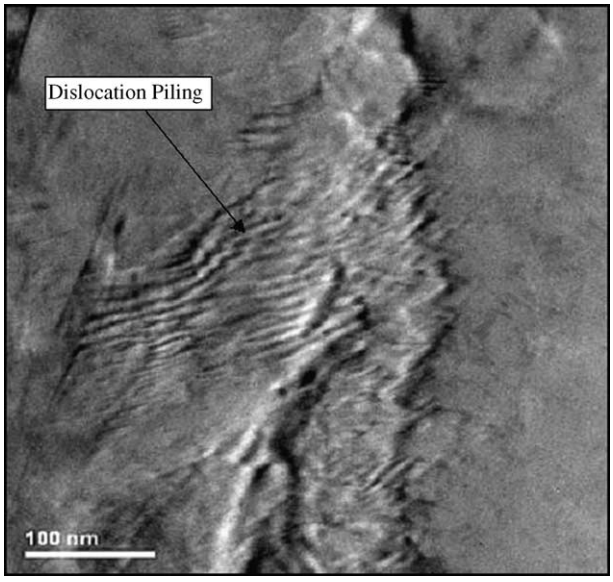

Fig. 9. 100 vol.% He processed coating showing dislocations arranging at interface.

stress accumulation within the deposition coating. Dislocation piling is clearly observed in isolated areas, corroborating strain hardening and higher stresses in the areas and thereby substantiating the higher hardness values observed for the 100 vol.% He processed coatings [15,18]. Dislocations, being high-energy areas, assist the polarization of the sites for increased corrosion activity under electrochemical experimentations. Hence a lower corrosion potential and a higher corrosion current is obviously expected for 100 vol.% He processed 1100 Al coating [3].

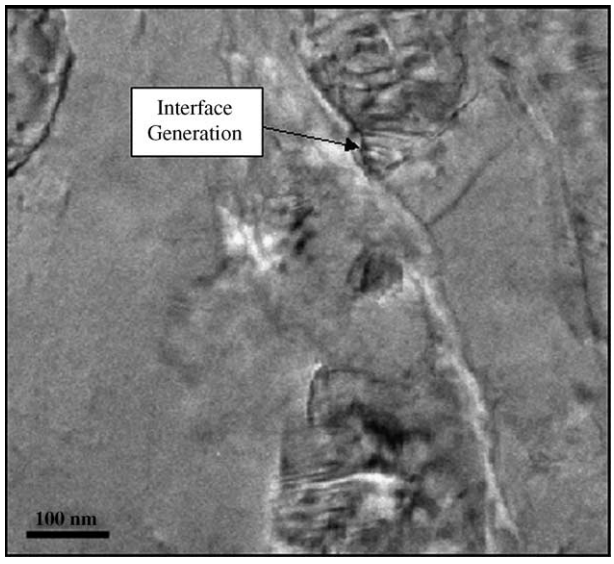

Fig. 10. He–20 vol.% N_2 processed coating showing formation of interfaces.

Fig. 10 displays the formation of grain boundaries in the substructure of the He–20 vol.% N_2 processed coating. Generation of the grain boundaries indicates that compressive stresses are relieved with the formation of interfaces and grains in the structure. Generally the energy expended in the deformation of material by cold working is converted to heat and some of it gets stored in the lattice. Since the dislocation cell structure is not thermodynamically stable, the microstructure softens and reverts to a strain-free state with time and temperature. Recrystallization of the structure with strain-free grains, an indication of replacement of the cold-worked structure, is clearly evidence of a decrease in hardness or strength and an increase in ductility in the He–20 vol.% N_2 processed 1100 Al coating [15,18]. High-energy areas resulting from stress, strain hardening and dislocation piling assist accelerated corrosion in 100 vol.% He-processed coating. Hence, the uniform structure and thin scattered oxide in He–20 vol.% N_2 coating displayed superior corrosion resistance when compared to that of 100 vol.% He cold sprayed coating.

4. Conclusion

Analytical scanning electron microscopy and transmission electron microscopy endorsed the structural characteristic correlation to micro hardness and electrochemical behavior. Helmholtz–Kelvin interface perturbations were more pronounced in He–20 vol.% N_2 processed coatings when compared to that of 100 vol.% He processed coatings. The shock wave pattern in 100 vol.% He processed coating displayed a higher degree of strain hardening, and a smooth interface transition between successive depositing splats. On the other

hand, the beach flow pattern in He–20 vol.% N_2 depicted more flattening of particles and reduced interface compatibility between cold sprayed splats. The oxide layer existence in 100 vol.% He processed coating showed an increased corrosion current density and reduced corrosion potential caused by concentration of polarization sites. Distributed oxide, shock wave structure, restrained flow lines and dislocation piling endorsed higher hardness of the 100 vol.% He processed coating. He–20 vol.% N_2 processed coating depicted subgrain formation, indicating lower hardness and endorsing stress relief structure.

Acknowledgements

Authors wish to acknowledge Dr. Y. Liu, Department of Mechanical and Materials Engineering, and Ms. B. Maloney, Earth Sciences Department, Florida International University, for their help with the SEM characterization. Authors sincerely thank AMPAC (Advanced Materials Process and Analysis Center), University of Central Florida, for carrying out TEM imaging.

References

[1] Papyrin AN, Alkimov AP, Kosarev VF. United Thermal Spraying Conference, Duesseldorf, Germany, 1999.
[2] McCune RC, Papyrin AN, Hall JN, Riggs II WL, Zajchowski PH. In: Proc. of 8th National Thermal Spraying Conference, Houston, TX, September 11–15, 1995: p. 1.
[3] Balani K, Laha T, Agarwal A, Karthikeyan J, Munroe N. Surf Coat Technol 2005;195(2–3):272.
[4] Smith MF, Brockmann JE, Dykhuizen RC, Gilmore DL, Neiser RA, Roemer TJ. Mater Res Soc Sym Proc 1999;542:65.
[5] Van Steenkiste TH, Smith JR, Teets RE, Moleski JJ, Gorkiewicz DW, Tison RP, et al. Surf Coat Technol 1999;111:62.
[6] Van Steenkiste TH, Smith JR, Teets RE. Surf Coat Technol 2002;154:237–52.
[7] Lima RS, Karthikeyan J, Kay CM, Lindemann J, Berndt CC. Thin Solid Films 2002;416:129.
[8] Grujicic M, Saylor JR, Beasley DE, DeRosset WS, Helfritch D. Appl Surf Sci 2003;219:211.
[9] Dykhuizen RC, Smith MF, Gilmore DL, Neiser RA, Jiang X, Sampath S. J Therm Spray Technol 1999;8(4):559.
[10] Li CJ, Li WY. Surf Coat Technol 2003;167(2–3):278.
[11] Perry RH, Green DW, editors. Perry's chemical engineers' handbook. 7th ed. McGraw-Hill, 1997.
[12] Dykhizen RC, Neiser RA. Thermal Spray. Advancing the science and applying the technology, vol. 1. Materials Park (OH): ASM International; 2003. p. 19.
[13] Agarwal A, McKechnie T, Seal S. J Therm Spray Technol 2003;12(3):350.
[14] Rea KE, Agarwal A, McKechnie T, Seal S. Microsc Res Tech 2005;66:10.
[15] Dieter GE. Mechanical metallurgy. Singapore: McGraw-Hill Series in Materials Science and Engineering; 2001.
[16] Li CJ, Li WY, Xian, Fukanuma H, Saitama J. In: Proceedings of the international thermal spraying conference 2004, May 10–12, 2004, Osaka, Japan. Düsseldorf, Germany: DVS-German Welding Society; 2004.
[17] Vlcek J, Zwick J, Huber H, Schnaut U, Lugscheider E, In: Proceedings of the international thermal spray conference 2002, Essen, Germany, March 4–6, 2002, Düsseldorf, Germany: DVS-German Welding Society; 2002.
[18] Gärtner F, Borchers C, Stoltenhoff T, Kreye H, Assadi H. Thermal spray. In: Marple BR, Moreau C, editors. Advancing the science and applying the technology. Materials Park (OH): ASM International; 2003. p. 1.